Journal of The Electrochemical Society, **157** (10) J342-J346 (2010)
0013-4651/2010/157(10)/J342/5/$28.00 © The Electrochemical Society

Luminescence and Spectroscopic Properties of Yellow-Emitting Carbonitride Phosphors and Their Application in White LEDs

Yun-Chen Wu,[a] Teng-Ming Chen,[a,*,z] Chuang-Hung Chiu,[b] and Chi-Neng Mo[b]

[a]*Phosphors Research Laboratory and Department of Applied Chemistry, National Chiao Tung University, Hsinchu 30010, Taiwan*
[b]*Chunghwa Picture Tubes Limited, Taoyuan 33444, Taiwan*

A series of yellow-emitting carbonitride phosphors with compositions of $(Y_{1-x}Ce_x)_2(CN_2)_3$ (x = 0–0.1) was synthesized by using exothermic solid-state metathesis reactions. The wavelength of the broad band yellow emission was tunable, varying from 570 to 577 nm. The photoluminescence (PL) intensity enhanced with increasing Ce^{3+} dopant content and was optimized at 3 mol % under excitation at 415 nm. We analyzed the 5d energy levels of Ce^{3+} in a capped trigonal prismatic complex and estimated the vibronic coupling parameters and Stokes shifts. To understand the thermal quenching behavior, the temperature-dependent PL for $(Y_{1.97}Ce_{0.03})_2(CN_2)_3$ was investigated. To demonstrate its potential application, we fabricated a warm white light-emitting diode (LED) using $(Y_{1.97}Ce_{0.03})_2(CN_2)_3$, pumped with a 420 nm GaInN LED chip, and the electroluminescence data were also presented.
 [DOI: 10.1149/1.3476307]

Manuscript submitted April 1, 2010; revised manuscript received July 14, 2010. Published August 19, 2010.

Recently, there has been growing interest in white light-emitting diodes (WLEDs) because of their energy-saving feature, high material stability, and long operation lifetime.[1] Thus, WLEDs are promising candidates and have been used to replace conventional incandescent and fluorescent lamps.[2] The white light can be generated by blue light-emitting diode (LED) chips and complementary yellow-emitting phosphor yttrium aluminum garnet:Ce^{3+}.[3] However, the disadvantages of this method are low color-rendering index and high color temperature due to the deficiency of the red emission in the visible spectrum. Rare-earth doped nitrides have been used to solve this problem in WLEDs and have gained much attention owing to their good thermal and chemical stabilities, low toxicity, and promising luminescence properties.[4] All-nitride multichromatic WLEDs are realized by integrating green-emitting β-SiAlON:Eu^{2+},[5] red-emitting $CaAlSiN_3$:Eu^{2+},[6] and $M_2Si_5N_8$:Eu^{2+} (M = Sr and Ba)[7-9] phosphors and a blue InGaN LED chip. Although a low color temperature property can be achieved, the mixed phosphor layer still suffers from aggregation from different sizes of phosphor particles and the reabsorption caused by a chromatic overlap of the phosphor blend. To overcome these problems, yellow-emitting phosphors with unisize and broad band emission such as Ca-α-SiAlON:Eu^{2+} [10,11] and $CaAlSiN_3$:Ce^{3+} [12] have been developed for fabricating dichromatic WLEDs, and a warm white light at color temperatures ranging from 1900 to 3700 K can be generated. In the present, most of the luminescence studies on rare-earth in solids have focused on silica- or silicon-based nitrides where luminescence centers are surrounded by the SiN_4 tetrahedral framework. These silicon-based nitrides have been synthesized using high pressure and high temperature procedures in the range from 1600 to 1900°C.[5-12] Recently, host materials containing cerium enclosed by carbodiimide (also called cyanamides) synthesized at lower temperature have been reported by Neukirch et al., such as $Re_2(CN_2)_3$ compounds with Re = Y, Ce–Nd, Sm, Gd–Lu.[13] Attributed to the influence of strong covalent interaction and crystal field splitting, the rare-earth doped carbonitride phosphors, such as $Gd_2(CN_2)_3$:Ce^{3+}, have been considered as novel host lattice materials, which exhibit longer excitation and emission wavelengths compared to their oxide counterparts.[14] Also, several families of rare-earth oxocarbodiimide compounds, such as $Re_2O_2(CN_2)$:Eu^{3+} (Re = Y, La, Gd), have been investigated for their similarity to red-light emitter Y_2O_2S:Eu^{3+}.[15] In this work, we revisited the low temperature synthetic route for a yellow-emitting Ce^{3+}-doped $Y_2(CN_2)_3$ phosphor and systematically investigated the structural and optical properties, the thermal influence on the luminescence characteristics of this phosphor, and the availability for fabrication of warm WLEDs.

Experimental

All manipulations of the starting materials were performed in a nitrogen-filled glove box (MBraun Unilab GmbH, Germany) due to the oxygen and moisture sensitivity of commercial and presynthesized starting materials $Li_2(CN_2)$, which were prepared from a finely ground mixture of Li_3N (Cerac Inc., purity 99.9%) and 1,3,5-triazine-2,4,6-triamine (Acros Organics, purity 99.5%) with a slight excess of 1,3,5-triazine-2,4,6-triamine according to the method reported by Neukirch et al.[13] The starting materials include YF_3 (Aldrich Chemicals, purity 99.9%), $Li_2(CN_2)$, and CeF_3 (Aldrich Chemicals, purity 99.99%).

In this work, a series of $(Y_{1-x}Ce_x)_2(CN_2)_3$ (x = 0, 0.005, 0.01, 0.03, 0.05, and 0.1) phosphors was prepared by employing an exothermic solid-state metathesis reaction. YF_3, $Li_2(CN_2)$, and CeF_3 were well mixed in stoichiometric molar ratio and loaded into an alumina tubing, which was readily transferred into a vertically positioned silica ampoule, fully evacuated, and sealed off under a dynamic vacuum. The silica ampoule was heated to 500–700°C at 2°C/min for 8–12 h and then cooled down slowly to room temperature. The products were washed with water and then dried with acetone. For temperatures higher than 800°C, the reaction products melted.

The chemical reaction can be summarized in the following

$$2(1-x)YF_3 + 3Li_2(CN_2) + 2x\ CeF_3 \rightarrow (Y_{1-x}Ce_x)_2(CN_2)_3 + 6LiF \quad [1]$$

The phase purity of the reaction product was analyzed by powder X-ray diffraction (XRD) using a Bruker AXS D8 advanced automatic diffractometer with Cu Kα radiation (λ = 1.5405 Å, 40 kV × 20 mA). The photoluminescence (PL) and photoluminescence excitation (PLE) spectra were obtained by using a Spex Fluorolog-3 spectrofluorometer equipped with a 450 W Xe light source and cutoff filters to avoid the second-order emission of the source radiation. The diffuse reflection (DR) spectra were measured with a Hitachi 3010 double-beam ultraviolet-visible (UV-vis) spectrometer (Hitachi Co., Tokyo, Japan). The Commission Internationale de l'Eclairage (CIE) chromaticity coordinates were determined by a Laiko DT-100 color analyzer equipped with a charge-coupled device detector (Laiko Co., Tokyo, Japan). The prototype LED devices were fabricated from commercial blue-violet InGaN LEDs (λ_{max} = 420 nm) with as-synthesized yellow-emitting $Y_2(CN_2)_3$:Ce^{3+} phosphors. The electroluminescence (EL) spectra

* Electrochemical Society Active Member.
z E-mail: tmchen@mail.nctu.edu.tw

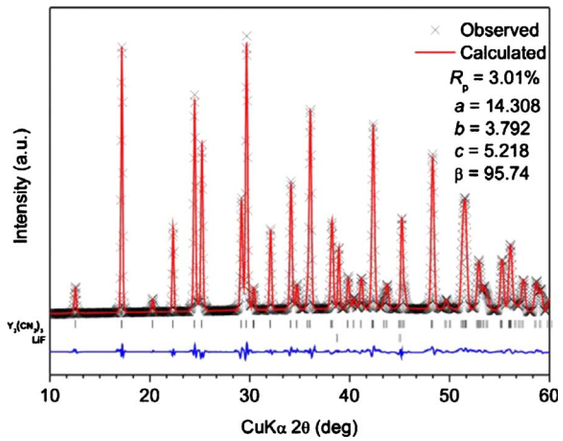

Figure 1. (Color online) Observed (cross) and calculated (red line) XRD patterns and the difference (blue line) between them. Bragg positions are shown as vertical bars.

were recorded under a forward bias of 5 V and a drive current of 350 mA and measured by using a 6 in. SphereOptics integrating sphere with LED measurement starter packages (Onset, Inc.).

Results and Discussion

Structural characterizations of $(Y_{0.97}Ce_{0.03})_2(CN_2)_3$ *phosphor.*— The XRD pattern (Fig. 1) of as-synthesized polycrystalline $(Y_{0.97}Ce_{0.03})_2(CN_2)_3$ was refined by using the General Structure Analysis System[16] software package. The Rietveld analysis results indicated the final weighted profile $R_p = 3.01\%$ and $R_{wp} = 4.15\%$, which revealed the presence of a dominant phase of $Y_2(CN_2)_3$ [13] and a secondary phase of coproduced LiF eutectics. The formed LiF played an important role as molten salt, which lowered the synthetic temperature and increased the crystallinity of the reaction product. As both Ce^{3+} and Y^{3+} ions were of the same valence, there was no charge compensation issue for isovalent substitution. $Y_2(CN_2)_3$ was isostructural with $Ln_2(CN_2)_3$ (Ln = Ce–Nd, Sm, Gd–Er) (ICSD CC no. 240312) having the *C*2/*m* space group, in which $(Y/Ce)^{3+}$ ions had one crystallographic position at the 4i sites without any site mixing. In occupancy parameters, the results were fitted to the nominal stoichiometry. As presented in Fig. 2, the unit cell was constructed by one layer of (Y^{3+}/Ce^{3+}) ions and one layer of $[NCN]^{2-}$ anions within the *c*-axis repeat. The (Y^{3+}/Ce^{3+}) ions were directly coordinated by seven N^{3-} ions crossing over two unit cells in the range of 2.6 Å. This polyhedral symmetry of the $(Y/Ce)^{3+}$ ion site could be described as capped trigonal prismatic where one of the N atom locates far away from the (Y/Ce) atoms. The oxygen content in the resultant carbonitride compound had been suppressed as low as possible by using pure raw materials and high vacuum processes. The amount of formed oxide impurities could affect the PL intensity and emission wavelength. The relative differences in the XRD peak intensities and diffraction angle (2θ), compared to those of pristine $Y_2(CN_2)_3$, were attributed to the incorporation of Ce^{3+} in $Y_2(CN_2)_3$. The lattice dimension of $Y_2(CN_2)_3$ was expected to expand because of the larger Ce^{3+} ion replacing the smaller Y^{3+} ion, which caused the 2θ angle to shift toward the lower angle direction, as presented in Fig. 1. The lattice parameters of the as-synthesized polycrystalline $(Y_{0.97}Ce_{0.03})_2(CN_2)_3$ has been refined as $a = 14.308(3)$ Å, $b = 3.792(3)$ Å, $c = 5.218(5)$ Å, and $\beta = 95.74(1)°$ compared to those [i.e., $a = 14.278(9)$ Å, $b = 3.781(6)$ Å, $c = 5.209(3)$ Å, and $\beta = 95.73(5)°$] of $Y_2(CN_2)_3$.[13]

Spectroscopic characterizations of $(Y_{1-x}Ce_x)_2(CN_2)_3$ *phosphor.*— The DR spectra of as-synthesized polycrystalline $(Y_{1-x}Ce_x)_2(CN_2)_3$ ($x = 0$, 0.01, 0.02, 0.03) phosphors are shown in Fig. 3a. To probe the absorbance of the host lattice, the Kubelka–Munk absorption coefficient (K/S) relation was used to calculate the measured reflectance (R) for all samples[17,18]

$$\frac{K}{S} = \frac{(1-R)^2}{2R} \qquad [2]$$

where K represents the absorption coefficient, S represents the scattering coefficient, and R represents reflectance. The fundamental absorption edge (bandgap energy) of the $Y_2(CN_2)_3$ host was calculated to be ~4.94 eV and was a very weak self-activated emitter under UV excitation. The light yellow to yellow body colors of $(Y_{1-x}Ce_x)_2(CN_2)_3$ were observed to be deepened with increasing Ce^{3+} dopant concentration. As indicated in Fig. 3b, the PLE spectra consist of three main bands (i.e., A, B, and C) in the UV-vis range, where band A centered at ~250 nm was attributed to the charge transfer between the Y^{3+} ion and N^{3-} ions of the CN_2^{2-} groups and the transition was related to the defects present in the host lattice. This observation was also consistent with that revealed in the DR spectra. The other two excitation bands (B and C) were attributed to the dipole-allowed transition from the lower fundamental $4f^1(^2F)$ electronic levels to the $5d^1(^2D)$ levels of the Ce^{3+} ion. The relative intensity of the two bands varied with doped Ce^{3+} concentration, which indicates the effect of optical absorption saturation. As indicated in Fig. 3b, we have also investigated the effect of Ce^{3+} dopant content optimization on the PL intensity of $(Y_{1-x}Ce_x)_2(CN_2)_3$ and an optimal $(Y_{0.97}Ce_{0.03})_2(CN_2)_3$ composition was determined. The PL spectra consisted of a single broad band extending from 440 to 800 nm with different maxima centered at 570–577 nm for $(Y_{1-x}Ce_x)_2(CN_2)_3$ samples with various x values. The asymmetric emission band in the PL spectra could be well fitted in a good approximation with two Gaussian curves centering at 545 and 614 nm, respectively, which could be ascribed to the transitions from the lowest 5d level to the two ground states $^2F_{5/2}$ and $^2F_{7/2}$ of the Ce^{3+} ions. The energy gap between $^2F_{7/2}$ and $^2F_{5/2}$ due to spin–orbit coupling was estimated to be ~2000 cm^{-1} (256 meV). In the carbonitride phosphor, the Y^{3+} ions were substituted by the Ce^{3+} ions and a strong yellow emission was observed, indicating that the Ce^{3+} ions

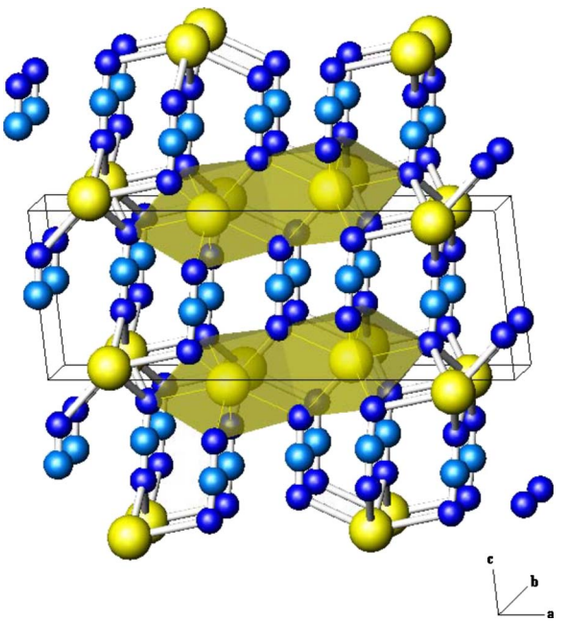

Figure 2. (Color online) Unit cell representation of $Y_2(CN_2)_3$:Ce (Y/Ce atom: Yellow sphere, N atom: Blue sphere, and C atom: Light blue sphere) and the shaded part highlights the capped trigonal prismatic coordination of Y/Ce atoms.

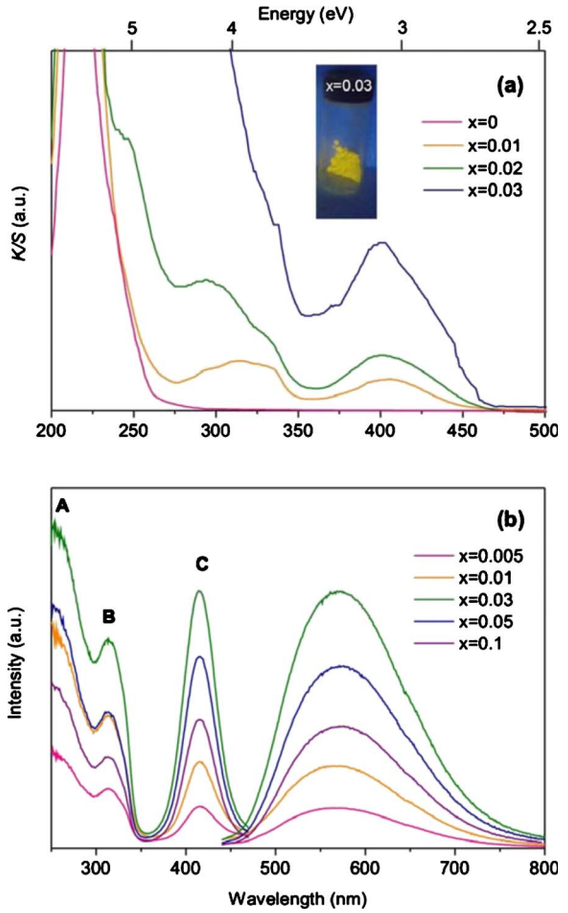

Figure 3. (Color online) (a) DR spectra and (b) excitation (λ_{ex} = 415 nm) and emission (λ_{em} = 570–577 nm) spectra of $(Y_{1-x}Ce_x)_2(CN_2)_3$ (x = 0.005, 0.01, 0.03, 0.05, 0.1) phosphors. The inset shows luminescence of $(Y_{0.97}Ce_{0.03})_2(CN_2)_3$ under 365 nm excitation.

preferred the trivalent state under the stated preparation conditions. As indicated in Fig. 3b, the wavelengths of the excitation bands in the PLE spectra were nearly the same; however, the emission spectra showed a slight redshift with increasing Ce^{3+} concentration. With increasing Ce^{3+} content, the PL intensity of $(Y_{1-x}Ce_x)_2(CN_2)_3$ reached a maximum at x = 0.03, and then concentration quenching occurred at $x > 0.03$. The full width at half-maximum of the emission band was larger than 120 nm, which implied that Ce^{3+}-doped $Y_2(CN_2)_3$ may achieve good color rendering when incorporated in LEDs.

In the $Y_2(CN_2)_3$ host lattice, the Ce^{3+} ion is located at the center of a capped trigonal prism formed by seven N^{3-} anions. With this C_{2v} symmetry, the five 5d orbitals were split into four levels in the increasing order of energy levels $d_{x^2-y^2}$, d_{xz}, d_{yz}, d_{z^2}, and d_{xy}, as illustrated in Fig. 4. The excitation band B at 315 nm correlated with the $4f^1 \rightarrow 5d^1$ (a_2, a_1, and b_2) transitions, and the excitation band C at ~415 nm was due to the $4f^1 \rightarrow 5d^1$ (b_1 and a_1) transitions. The center of gravity of the excitation bands was calculated to be $\sim 28.81 \times 10^3$ cm^{-1}. Furthermore, based on the highest and lowest absorption bands in the PLE spectra shown in Fig. 4, the crystal field splitting was estimated to be $\sim 1.03 \times 10^4$ cm^{-1} (1.27 eV). Furthermore, we assumed that both the ground state $4f^1$ and the excited state $5d^1$ have parabolas with the same curvature and have almost equal energy of phonon in the configurational coordinate diagram. Then, the deconvoluted PL spectra may be well fitted with the following equation of Pekarian spectral distribution function $F(n)$ [19,20]

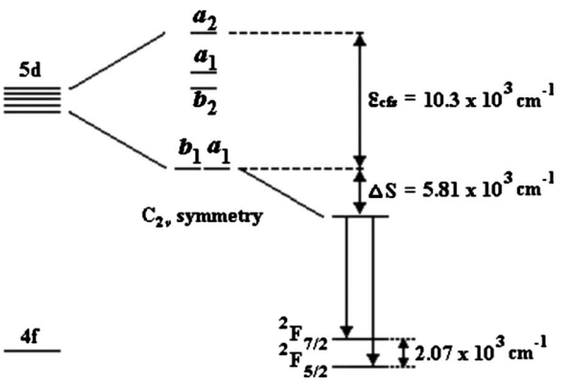

Figure 4. Crystal field splitting of the five 5d orbitals in a capped trigonal prismatic (C_{2v}) symmetry.

$$F(n) = \frac{e^{-S}S^n}{n!}\left[1 + S^2\frac{1}{(n+1)}e^{-\hbar\omega/kT}\right] \quad [3]$$

where S represents the Pekar–Huang–Rhys factor, the mean number of the photons with optical transitions, k represents Boltzmann's constant, and $\hbar\omega$ represents the vibronic level. The best fitting of the emission band was obtained with S = 3 and $\hbar\omega$ = 1170 cm^{-1} (145 meV), and the Stokes shift (ΔS) was also determined from $\Delta S = (2S - 1)\hbar\omega$ to be 5.85×10^3 cm^{-1}. These results were similar to that (i.e., 5.73×10^3 cm^{-1}) calculated from the empirical formalism proposed by Dorenbos.[21]

Thermal quenching property of $(Y_{1-x}Ce_x)_2(CN_2)_3$ phosphor.— The temperature-dependent PL spectra of $(Y_{0.97}Ce_{0.03})(CN_2)_3$ were also investigated in the range of 25–250°C, and the PL spectra are shown in Fig. 5. As shown in Fig. 6a, as the temperature increased, the PL intensity diminished compared to that of the same sample observed at 25°C, which may be rationalized in terms of the increased thermal energy utilized to excite electrons to the bottom of the conduction band and then ionized.[12] As indicated in Fig. 6a, it was also observed that the wavelength of the Ce^{3+} emission exhibited mainly a redshift for $(Y_{1-x}Ce_x)(CN_2)_3$ with $x < 0.02$ and a blueshift for those with $x > 0.02$. The observed redshifting could presumably be explained by the temperature-induced structural relaxation and an increased Stokes shift.[12] In contrast, the blueshifting was the result of the energy transfer between Ce^{3+} ions.[22] To understand the origin of temperature-dependent emission intensity $I(T)$,

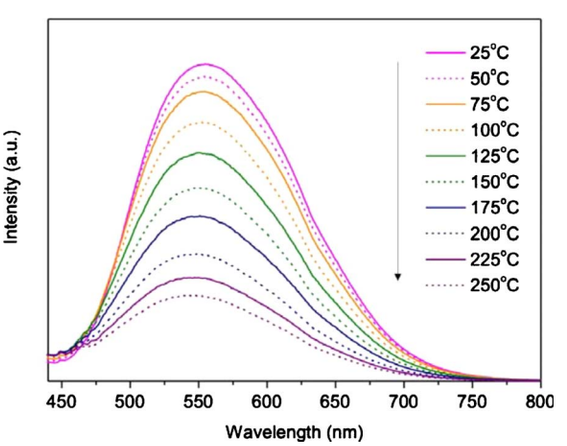

Figure 5. (Color online) Temperature dependence of PL spectra of $(Y_{0.97}Ce_{0.03})_2(CN_2)_3$ excited at 415 nm.

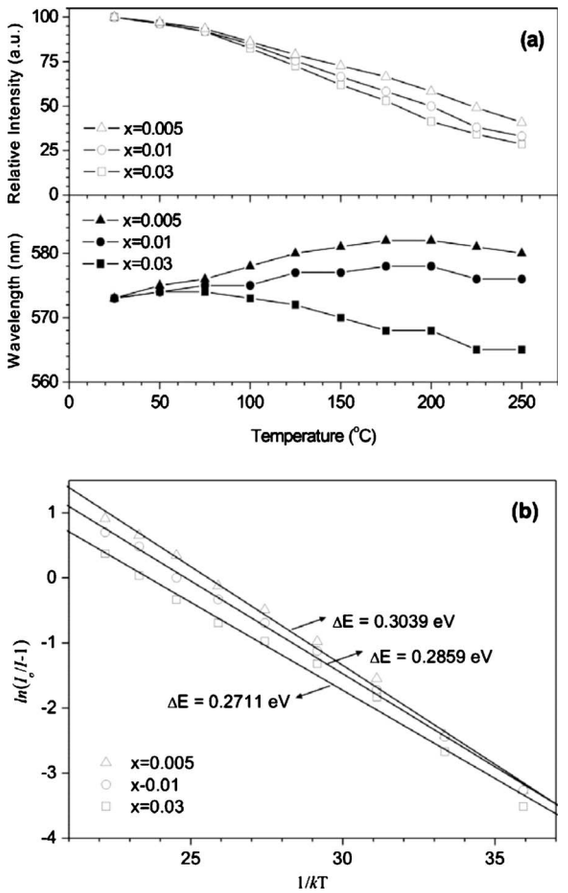

Figure 6. (a) Temperature dependence of PL intensity and λ_{em} of $(Y_{1-x}Ce_x)_2(CN_2)_3$ (x = 0.005, 0.01, 0.03) under excitation at 415 nm. (b) The fitted PL intensity and the calculated thermal activation energy (ΔE) as a function of temperature.

the activation energy (E_a) of the electrons excited from the 4f states to the lowest 5d states of Ce^{3+} can be described in the following equation[23]

$$I(T) = \frac{I_o}{1 + A\ \exp\left(-\frac{E_a}{kT}\right)} \qquad [4]$$

where I_0 and $I(T)$ represent the PL intensity at room temperature and any temperature, respectively, and k represents Boltzmann's constant. The values of E_a for $(Y_{1-x}Ce_x)_2(CN_2)_3$ with x = 0.005, 0.01, and 0.03 were calculated to be 0.3039, 0.2859, and 0.2711 eV, respectively, as indicated in Fig. 6b. Therefore, with increasing Ce^{3+} concentration, the thermal energy increased and could excite more electrons to the 5d states of the Ce^{3+} ions due to the lower activation energy.

Performance of WLEDs based on $(Y_{0.97}Ce_{0.03})_2(CN_2)_3$ phosphor.— To demonstrate its potential application, we have fabricated a series of phosphor-converted WLEDs by using a phosphor blend containing $(Y_{0.97}Ce_{0.03})_2(CN_2)_3$ combined with a 420 nm GaInN LED chip. The phosphor blend was formed by dispersing the carbonitride phosphor in 10, 15, 20, and 25 wt % in a transparent silicone resin, and the devices were then fabricated by coating the LED chips with epoxy resin. Figure 7 shows the EL spectrum with various phosphor contents, and the whole visible spectral region could be achieved when excited by the violet-blue LED, as indicated in Fig. 7. The color-rendering index (Ra) of this dichromatic WLED was

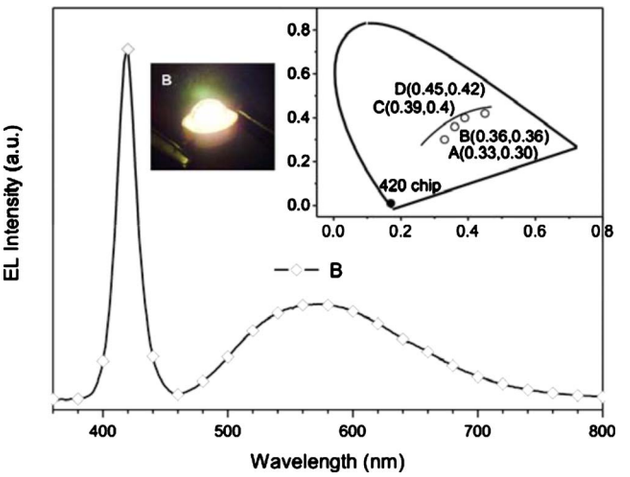

Figure 7. (Color online) EL spectra and the appearance of a warm WLED fabricated using $Y_2(CN_2)_3:Ce^{3+}$ pumped with a 420 nm near-UV LED chip under a forward bias of 5 V and current of 350 mA. The inset shows the variation in CIE chromaticity coordinates as a function of fraction of phosphor used.

determined to be around 70. As represented in the inset of Fig. 7, the CIE chromaticity coordinates of the $(Y_{0.97}Ce_{0.03})_2(CN_2)_3$ phosphor, the chip and WLEDs were (0.48, 0.50), (0.17, 0.01), A (0.33, 0.30), B (0.36, 0.36), C (0.39, 0.40), and D (0.45, 0.42), respectively. The corresponding color temperature of points A–D ranging from 4500 to 2500 K could be achieved by tuning the chromaticity contribution from the $(Y_{0.97}Ce_{0.03})_2(CN_2)_3$ phosphor. The corresponding experimental luminous efficiencies were 7.2, 6.6, 5.9, and 5.1 lm/W for the four WLEDs with chromaticity represented by points A, B, C, and D, respectively (inset of Fig. 7). The dichromatic WLED could avoid the problem of aggregation from different phosphor particle sizes and possible reabsorption from chromatic overlap. However, the lack of green and red regions in the fabricated WLEDs apparently abated the performance of color rendering. Undoubtedly, the Ra value could be improved by blending with other phosphors; however, the choice of phosphors with homogeneous and narrow particle size distribution and the optimization of different phosphors should be considered.

Conclusion

In summary, a series of yellow-emitting carbonitride phosphors $(Y_{1-x}Ce_x)_2(CN_2)_3$ (x = 0.005–0.1) was synthesized and investigated. The PL/PLE spectra, chromaticity, thermal quenching, and device performance were investigated and presented. The emission wavelength of the broad band yellow was tunable, varying from 570 to 577 nm, and the PL intensity enhanced with increasing Ce^{3+} dopant content and was optimized at 3 mol % under excitation at 415 nm. To demonstrate its potential application, we fabricated a warm WLED using $(Y_{1.97}Ce_{0.03})_2(CN_2)_3$, pumped with a 420 nm GaInN LED chip, and the EL data were presented.

Acknowledgments

The authors thank the members of Professor Chi-Shen Lee at NCTU for their assistance with the structural refinement. This research was supported by the Chunghwa Picture Tubes Limited of Taiwan and, in part, by the National Science Council of Taiwan under contract no. NSC98-2113-M-009-005-MY3.

National Chiao Tung University assisted in meeting the publication costs of this article.

References

1. S. Nakamura, T. Mukai, and M. Senoh, *Appl. Phys. Lett.*, **64**, 1687 (1994).
2. T. Hashimoto, F. Wu, J. S. Speck, and S. Nakamura, *Nature Mater.*, **6**, 568 (2007).

3. Y. X. Pan, M. M. Wu, and Q. Su, *J. Phys. Chem. Solids*, **65**, 845 (2004).
4. W. Schnick, *Int. J. Inorg. Mater.*, **3**, 1267 (2001).
5. N. Hirosaki, R.-J. Xie, K. Kimoto, T. Sekiguchi, Y. Yamamoto, T. Suehiro, and M. Mimoto, *Appl. Phys. Lett.*, **86**, 211905 (2005).
6. X. Piao, K. Machida, T. Horikawa, H. Hanzawa, Y. Shimomura, and N. Kijima, *Chem. Mater.*, **19**, 4592 (2007).
7. R.-J. Xie, N. Hirosaki, T. Suehiro, F.-F. Xu, and M. Mimoto, *Chem. Mater.*, **18**, 5578 (2006).
8. X. Piao, T. Horikawa, H. Hanzawa, and K. Machida, *Appl. Phys. Lett.*, **88**, 161908 (2006).
9. M. Zeuner, F. Hintze, W. Schnick, and H. Hanzawa, *Chem. Mater.*, **21**, 336 (2009).
10. R.-J. Xie, N. Hirosaki, K. Sakuma, Y. Yamamoto, and M. Mitomo, *Appl. Phys. Lett.*, **84**, 5404 (2004).
11. H. L. Li, R.-J. Xie, N. Hirosaki, T. Suehiro, and Y. Yajima, *J. Electrochem. Soc.*, **155**, J175 (2008).
12. Y.-Q. Li, N. Hirosaki, R.-J. Xie, T. Takeda, and M. Mitomo, *Chem. Mater.*, **20**, 6704 (2008).
13. M. Neukirch, S. Tragl, and H.-J. Meyer, *Inorg. Chem.*, **45**, 8188 (2006).
14. J. Glaser, L. Unverfehrt, H. Bettentrup, G. Heymann, and H. Huppertz, T. Jüstel, and H.-J. Meyer, *Inorg. Chem.*, **47**, 10455 (2008).
15. J. Sindlinger, J. Glaser, H. Bettentrup, T. Jüstel, and H.-J. Meyer, *Z. Anorg. Allg. Chem.*, **633**, 1686 (2007).
16. A. C. Larson and R. B. Von Dreele, General Structure Analysis System (GSAS), Los Alamos National Laboratory Report LAUR 86–748, Los Alamos National Laboratory (1994).
17. P. Kubelka and F. Munk, *Z. Tech. Phys. (Leipzig)*, **12**, 593 (1931).
18. Y.-I. Kim, K. Page, A. M. Limarga, D. R. Clarke, and R. Seshadri, *Phys. Rev. B*, **76**, 115204 (2007).
19. M. Nazarov, D.-Y. Noh, C.-C. Byeon, and H. Kim, *J. Appl. Phys.*, **105**, 073518 (2009).
20. M. Nazarov, B. Tsukerblat, and D. Y. Noh, *J. Lumin.*, **128**, 1533 (2008).
21. P. Dorenbos, *J. Lumin.*, **91**, 155 (2000).
22. Y. Q. Li, N. Hirsaki, R. J. Xie, and M. Mimoto, *Sci. Technol. Adv. Mater.*, **8**, 607 (2007).
23. R.-J. Xie, N. Hirosaki, N. Kimura, K. Sakuma, and M. Mitomo, *Appl. Phys. Lett.*, **90**, 191101 (2007).